

Sequential Residual-Based RAIM

Mathieu Joerger and Boris Pervan,
Illinois Institute of Technology

BIOGRAPHY

Dr. Mathieu Joerger obtained a Master in Mechatronics from the National Institute of Applied Sciences in Strasbourg, France, in 2002. He pursued studies in Mechanical and Aerospace Engineering at the Illinois Institute of Technology (IIT) in Chicago, where he earned a M.S. degree in 2002, and a Ph.D. in 2009. He is the 2009 recipient of the ION Bradford Parkinson award, which honors outstanding graduate students in the field of GNSS. Mathieu is currently working as a research associate at the Illinois Institute of Technology on the integration of GPS with laser scanners, and on multi-constellation navigation satellite systems for high-integrity precision applications.

Dr. Boris Pervan is Professor of Mechanical and Aerospace Engineering at the Illinois Institute of Technology (IIT), where he conducts research on high-integrity satellite navigation systems. Prof. Pervan received his B.S. from the University of Notre Dame, M.S. from the California Institute of Technology, and Ph.D. from Stanford University. Prior to joining the faculty at IIT, he was a spacecraft mission analyst at Hughes Space and Communications Group and was project leader at Stanford University for GPS LAAS research and development. He was the recipient of the Mechanical and Aerospace Dept. Excellence in Research Award (2007), IIT/Sigma Xi Excellence in University Research Award (2005), University Excellence in Teaching Award (2005), Ralph Barnett Mechanical and Aerospace Dept. Outstanding Teaching Award (2002, 2009), IEEE Aerospace and Electronic Systems Society M. Barry Carlton Award (1999), RTCA William E. Jackson Award (1996), Guggenheim Fellowship (Caltech 1987), and Albert J. Zahm Prize in Aeronautics (Notre Dame 1986). He is currently Editor of the ION journal Navigation.

ABSTRACT

This paper explores receiver autonomous integrity monitoring (RAIM) for sequences of filtered measurements. Optimal position estimation for navigation systems with known dynamics (such as carrier phase positioning or integrated GPS/INS navigation) is

provided by filtering measurements over time. All measurements within the time-sequence are vulnerable to faults. There is currently no widely implemented algorithm for the detection of faults that last over multiple epochs. In this work, two sequential residual-based RAIM algorithms are investigated. The first algorithm is a batch-type procedure. The batch least-squares residual is computed at each epoch using a sliding-window mechanism. It is derived in a compact formulation using a forward-backward smoother (FBS). The iterative FBS residual generation process includes a residual norm weighting procedure accounting for measurement error correlation and prior knowledge of state variables. The second method, based on a Kalman filter (KF), is truly sequential. A KF detection test statistic is defined and its probability distribution is established (assuming time-uncorrelated normally distributed measurement noise). The KF RAIM residual is carefully derived to enable probability of missed-detection determination at each time step. In addition, in contrast to the KF implementation, the sampling interval within the batch may be treated as an extra navigation design parameter: increasing the batch sampling interval decreases the estimation performance but lowers the batch computation load. In this research, the fault-detection performance sensitivity to sampling interval is investigated. The analysis yields counter-intuitive results in the presence of time-correlated measurement errors. Finally, both batch and KF residual-based RAIM methods are evaluated for a benchmark application of aircraft precision approach, where differential GPS and Galileo code and carrier phase measurements are filtered for floating cycle ambiguity estimation.

I. INTRODUCTION

This paper describes the design, analysis and evaluation of two sequential residual-based receiver autonomous integrity monitoring (RAIM) methods for navigation systems that involve measurement filtering over time. The first algorithm is a batch-type procedure. The batch least-squares weighted residual is computed at each epoch using a finite sequence of current and stored past-time measurements. The second method is based on a Kalman filter (KF). The KF RAIM residual is defined and its weighted norm is used as a RAIM test statistic to compute

the probability of missed-detection at each time step. Both algorithms are employed with carrier phase satellite ranging measurements, which require filtering over time for (floating) cycle ambiguity estimation. The potential high-integrity positioning performance of future carrier phase multi-constellation navigation systems is evaluated for applications in civil aviation.

The concept of RAIM was formalized in the late 1980's [1] [2]. It aims at achieving self-contained fault-detection at the user receiver by verifying the consistency of the over-determined positioning solution using redundant measurements. Multiple approaches toward RAIM have emerged over the past two decades (including residual-based techniques and range and position-domain solution separation methods) [3]. Most existing implementations of RAIM are 'snapshot' detection schemes that assume redundant observations at one epoch of interest. Snapshot RAIM is a natural choice for punctual (e.g., code-based) position fixes.

However, optimal position estimation often requires measurement filtering over multiple epochs. This is the case for dynamic navigation systems whose state propagation over time can be reliably modeled. For example, carrier phase cycle ambiguity states are known to be constant biases for as long as the signal is continuously tracked. Measurement filtering can also enable integration of dead-reckoning sensors such as inertial navigation systems (INS) [4], of laser scanner observations [5], of prior knowledge on receiver clock variations [6], and of vehicle dynamic models [7].

In this type of implementation, observations collected within the filtering interval are all vulnerable to rare-event integrity threats such as user equipment and satellite failures. When trying to protect the system against such faults (which may last in time), snapshot RAIM is limited in that the fault profile over time is never considered. Integrity budget allocation and conservative accounting of potentially undetected faults at previous epochs make consecutive snapshot RAIM checks cumbersome. Therefore, several methods have been published that aim at monitoring faults affecting successive measurements. Existing sequential fault detection algorithms for the most part only target specific fault modes [8], and their formulation and implementation is complex (e.g., banks of Kalman filters whose number increases with the number of epochs under consideration [9]). Of particular emphasis in this work, most existing sequential methods are not self-evaluating [10], which means that they do not assess their fault detection performance (e.g., in the form of a probability of missed detection).

In response, in our previous research [11], the detection of faults affecting a finite sequence of observations was achieved using a non-failure-specific residual-based

RAIM procedure. The method is similar to the well-established snapshot RAIM, but it is used for batches of measurements collected within a finite window in time. The concept is applicable to solution-separation: however for practical reasons, in order to avoid generating subset-solutions for each one of the numerous fault modes (as required in solution-separation), the residual-based procedure was preferred. Also, for algorithm evaluation, threat models were devised including realistic fault modes (impulses, steps and ramps of all magnitudes and start-times) as well as theoretical worst-case fault profiles, which maximize the probability of missed-detection (by maximizing the failure mode slope) for single or multiple satellite faults [12]. Least-squares batch implementation is compatible with real-time implementations using a sliding-window mechanism, provided that sufficient computation and memory capacity are available for the storage and processing of past-time measurements and state coefficients.

In this paper, a computationally-efficient iterative forward-backward smoother (FBS) equivalent to the least-squares batch implementation is employed. An associated method is established to compute the weighted norm of the residual; it accounts for measurement error time-correlation and prior knowledge of state variables. In parallel, a truly sequential KF-based procedure is devised (at this stage of the research, assuming time-uncorrelated normally distributed measurement noise). It outputs estimate errors and test statistics at each time step. The weighted norm of the KF RAIM residual (which serves as test statistic) is carefully derived to enable the computation of the probability of hazardous misleading information.

Unlike the KF procedure, the batch offers an extra degree of freedom in the selection of the sampling interval between stored past-time measurements. (The sampling interval within the batch does not need to be the same as the positioning update period.) Increasing the batch sampling interval decreases the estimation performance but lowers the batch computation load. The paper analyzes the fault-detection performance sensitivity to sample rate, which yields counter-intuitive results in the presence of measurement error correlation.

The integrity monitoring performance of both algorithms is evaluated for a benchmark application of aircraft precision approach. The proposed batch-type and KF-based RAIM procedures are evaluated against multiple fault profiles, for sequences of measurements collected over a fixed filtering period and for numerous satellite geometries. Sensitivity to the batch sampling interval is quantified. Finally, the fault-detection performance of both methods is assessed for a multi-constellation carrier-phase based navigation system, at multiple locations over the Contiguous United States (CONUS).

II. BACKGROUND ON SNAPSHOT RAIM

This section describes the well-established snapshot residual-based RAIM method and emphasizes fundamental principles that will be extended to multiple epochs in the following sections.

Estimation and Detection

Fault-detection using RAIM consists in verifying the consistency of an over-determined position solution using redundant observations. Let m and n respectively be the numbers of states and measurements at a single instant in time. Measurement redundancy implies:

$$n > m$$

Consider a vector \mathbf{z} of n stacked measurements that can be expressed as a linear function of a state vector \mathbf{x} , an observation matrix \mathbf{H} , a measurement noise vector \mathbf{v} and a fault vector \mathbf{f} (to be detected):

$$\mathbf{z} = \mathbf{H}\mathbf{x} + \mathbf{v} + \mathbf{f} \quad (1)$$

Vector \mathbf{v} is assumed normally distributed with zero mean and covariance matrix \mathbf{V} . We use the notation:

$$\mathbf{v} \sim \mathcal{N}(\mathbf{0}, \mathbf{V})$$

We also use the notation:

$$\begin{aligned} \boldsymbol{\varepsilon} &= \mathbf{v} + \mathbf{f}, \\ \boldsymbol{\varepsilon} &\sim \mathcal{N}(\mathbf{f}, \mathbf{V}) \end{aligned} \quad (2)$$

In snapshot RAIM, the n -dimensional measurement space is separated into two subspaces: the m -dimensional state space and the $(n-m)$ -dimensional parity space. RAIM methods quantify the impact of the fault \mathbf{f} (a) on the state estimate and (b) on a detection test statistic, derived from the parity vector (or equivalently from the residual vector).

First, the least-squares state estimate vector $\hat{\mathbf{x}}$ of \mathbf{x} , with covariance matrix $\mathbf{P}_{\hat{\mathbf{x}}}$, is given by:

$$\begin{aligned} \hat{\mathbf{x}} &= \mathbf{S}\mathbf{z} \\ \mathbf{P}_{\hat{\mathbf{x}}} &= (\mathbf{H}^T \mathbf{V}^{-1} \mathbf{H})^{-1} \end{aligned} \quad (3)$$

where \mathbf{S} is the pseudo-inverse of the observation matrix \mathbf{H} weighted by \mathbf{V}^{-1} :

$$\mathbf{S} = (\mathbf{H}^T \mathbf{V}^{-1} \mathbf{H})^{-1} \mathbf{H}^T \mathbf{V}^{-1} \quad (4)$$

The state estimate error $\delta\mathbf{x}$ is defined as:

$$\delta\mathbf{x} \equiv \hat{\mathbf{x}} - \mathbf{x} = \mathbf{S}\boldsymbol{\varepsilon} \quad (5)$$

RAIM analysis often focuses on a subset or on a linear combination of states, noted δx (e.g., focus on the vertical position coordinate for aircraft approach applications). The scalar δx can be expressed as:

$$\delta x = \mathbf{T}_x^T \delta\mathbf{x}$$

where \mathbf{T}_x is a $m \times 1$ vector of state coefficients (e.g., zeros and one to extract the vertical position coordinate). We have:

$$\delta x \sim \mathcal{N}(\mu_f, \mathbf{T}_x^T \mathbf{P}_{\hat{\mathbf{x}}} \mathbf{T}_x) \quad (6)$$

where the mean μ_f is a function of the fault \mathbf{f} :

$$\mu_f = \mathbf{T}_x^T \mathbf{S} \mathbf{f}. \quad (7)$$

Second, the residual \mathbf{r} is defined as:

$$\mathbf{r} \equiv \mathbf{z} - \mathbf{H}\hat{\mathbf{x}} \quad (8)$$

The norm of \mathbf{r} weighted by \mathbf{V}^{-1} is the RAIM detection test statistic:

$$\|\mathbf{r}\|_w^2 = \mathbf{r}^T \mathbf{V}^{-1} \mathbf{r} \quad (9)$$

It follows a non-central chi-square distribution with $n-m$ degrees of freedom and non-centrality parameter λ_f^2 (function of the fault vector \mathbf{f}):

$$\|\mathbf{r}\|_w^2 \sim nc \chi^2(n-m, \lambda_f^2) \quad (10)$$

$$\lambda_f^2 = \mathbf{f}^T \mathbf{V}^{-1} (\mathbf{I} - \mathbf{H}\mathbf{S}) \mathbf{f} \quad (11)$$

where \mathbf{I} is the identity matrix of appropriate dimensions.

Particularly relevant to this work is the fact that the random parts of the state estimate $\hat{\mathbf{x}}$ and of the residual \mathbf{r} are derived from orthogonal components of the measurement noise vector \mathbf{v} [13] [14]. It means that the random parts of $\hat{\mathbf{x}}$ and \mathbf{r} are *statistically independent*, which is instrumental when computing the probability of missed detection.

Computing the Probability of Missed Detection

RAIM requirements are specified for the estimate error and test statistic. The estimate error δx is compared to an alert limit AL . The test statistic $\|\mathbf{r}\|_w$ is evaluated against a threshold R_c , which is set in compliance with a continuity risk requirement P_c [13] (in order to limit the probability of false alarms).

These requirements define a probability of missed detection P_{MD} , which is the joint probability of the measurement error and fault $\boldsymbol{\varepsilon}$ causing hazardous conditions ($\delta x > AL$) with no detection ($\|\mathbf{r}\|_w < R_c$):

$$P_{MD} = P(\delta x > AL, \|\mathbf{r}\|_w < R_c)$$

If the random parts of δx and $\|\mathbf{r}\|_w$ are *statistically independent*, P_{MD} can be computed as a product of probabilities:

$$P_{MD} = P(\delta x > AL) P(\|\mathbf{r}\|_w < R_c) \quad (12)$$

P_{MD} can then be compared to the integrity risk requirement (or probability requirement of hazardous misleading information P_{HMI}):

$$P_{MD} < P_{HMI} / P_p \quad (13)$$

where P_p is the prior probability of fault occurrence.

Therefore, the independence condition between random parts of δx and $\|\mathbf{r}\|_w$ is crucial to enable P_{MD} computation and detection performance evaluation. Verifying this independence condition is a major concern when deriving sequential RAIM algorithms in the next two sections.

Failure Mode Plot

The impact of measurement errors and faults $\boldsymbol{\varepsilon}$ can be represented on a plot of δx versus $\|\mathbf{r}\|_w$. The y and x axes in Fig. 1 are respectively normalized by AL and R_C . The graph's upper left quadrant corresponds to the missed-detection area. An example failure \mathbf{f} defines a point on the plane, i.e., a value of the mean μ_f of δx and of the non-centrality parameter λ_f^2 of $\|\mathbf{r}\|_w^2$. Varying the fault magnitude describes a line passing through the origin, so that for a given fault mode, there is an associated slope parameter, noted *slope* in upcoming derivations. Finally, the normal and non-central chi-square distributions of respectively δx and $\|\mathbf{r}\|_w$ produce ovoid-shaped contours of constant joint probability density [11], one of which is schematically represented by an ellipse in Fig. 1 for an example failure mode \mathbf{f} .

In the following sections, algorithm analyses include comparisons of non-centrally chi-square distributed test statistics $\|\mathbf{r}\|_w$ with different numbers of degrees of freedom. To facilitate such comparisons, the x axis in Fig. 1 was normalized by the threshold R_C . R_C^2 is defined as the value for which the chi-square cumulative distribution function (CDF) with $n-m$ degrees of freedom equals $1-P_C$ [13]. Therefore, normalizing the x-axis by R_C yields a constant threshold of 1 for any number of degrees of freedom.

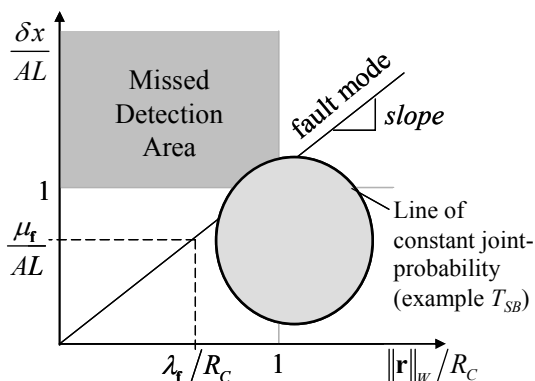


Fig. 1 Failure Mode Plot

III. PROBLEM STATEMENT: SEQUENTIAL ESTIMATION AND FAULT-DETECTION

Snapshot RAIM has been derived in various formulations and has been effectively implemented over decades [1] [3] [14] [15]. In this work, it is used as a foundation to derive sequential algorithms.

Consider two measurement equations at epochs 1 and 2 (subscripts 1 and 2), as well as a state time-propagation equation between the two epochs.

$$\mathbf{z}_1 = \mathbf{H}_1 \mathbf{x}_1 + \boldsymbol{\varepsilon}_1$$

$$\mathbf{z}_2 = \mathbf{H}_2 \mathbf{x}_2 + \boldsymbol{\varepsilon}_2$$

$$\mathbf{x}_2 = \boldsymbol{\Phi}_1 \mathbf{x}_1 + \mathbf{w}_1$$

where $\boldsymbol{\Phi}_1$ is the state propagation matrix and \mathbf{w}_1 the process noise vector.

The estimator provides state estimates $\hat{\mathbf{x}}_1$ and $\hat{\mathbf{x}}_2$ at both epochs, but, for real-time navigation purposes, the focus is usually on the current-time position estimate $\hat{\mathbf{x}}_2$. In parallel, the residual \mathbf{r} has components \mathbf{r}_1 and \mathbf{r}_2 , both of which might contribute to the test statistic and hence, might contribute to enhanced fault-detection performance.

Therefore, whereas only current-time state estimates are of interest, past-time residuals may be valuable, but only under the essential condition that the resulting residual-based RAIM test statistic remains statistically independent from the state estimate (to enable P_{MD} computation using equation 12).

To explore this concept, three estimation algorithms are considered. They are illustrated in Fig. 2 for a time sequence t_1 to t_q (t_q being the current time), over a sampling window T_{SW} . For any epoch k , the capital subscript K designates epochs 1 to k (i.e., for the current epoch q , Q designates all sample times over the entire smoothing window T_{SW}).

- Using a batch estimator, measurements \mathbf{z}_1 to \mathbf{z}_q are collected and stacked in a large measurement vector. They are processed at t_q using large state coefficient and weighting matrices. They provide optimal state estimates at each epoch knowing all measurements:

$$\hat{\mathbf{x}}_{q|Q} = [\hat{\mathbf{x}}_{1|Q}^T \cdots \hat{\mathbf{x}}_{q|Q}^T]^T$$

- The Kalman filter (KF) is truly sequential. It provides state estimates $\hat{\mathbf{x}}_{k|K}$ at each epoch using all *previous* measurements (as compared to $\hat{\mathbf{x}}_{k|Q}$ for the batch). At current time t_q , the KF state estimate $\hat{\mathbf{x}}_{q|Q}$ is identical to the batch, but processing involves smaller size matrices.

- The forward backward smoother (FBS) is a compact formulation of the batch. It consists of a KF over T_{SW} , followed by a backward smoothing step performed at t_q . It provides states estimates $\hat{\mathbf{x}}_{k|q}$ at each epoch knowing all measurement (identical to the batch at all epochs). However, it is computationally more efficient than a batch since the size of FBS matrices is the same as matrices used in KF processing.

The next section (Section IV) describes the batch RAIM residual and a procedure to compute weighted FBS residuals. Section V establishes a KF test-statistic and defines its probability distribution.

IV. BATCH RAIM RESIDUAL

The least-squares batch residual-based RAIM method is a direct extension of snapshot RAIM which uses sequences of measurements as input. Since snapshot and batch RAIM are well understood, the batch implementation is used as a reference when deriving weighted FBS and KF RAIM residuals.

Batch Least-Squares Residual-Based RAIM

At the current time step t_q , the sequence of measurements \mathbf{z}_1 to \mathbf{z}_q is arranged in a batch equation:

$$\begin{bmatrix} \mathbf{z}_1 \\ \vdots \\ \mathbf{z}_q \end{bmatrix} = \begin{bmatrix} \mathbf{H}_1 \\ \vdots \\ \mathbf{H}_q \end{bmatrix} \mathbf{x}_Q + \begin{bmatrix} \boldsymbol{\varepsilon}_1 \\ \vdots \\ \boldsymbol{\varepsilon}_q \end{bmatrix} \quad (14)$$

	Sampling Window T_{SW}					
Time epochs	t_1	t_2	...	t_k	...	t_q
Measurements (and state coeff.)	\mathbf{z}_1	\mathbf{z}_2	...	\mathbf{z}_k	...	\mathbf{z}_q
Batch						$\hat{\mathbf{x}}_{Q Q}$
Kalman filter (KF)	$\hat{\mathbf{x}}_{1 1}$	$\hat{\mathbf{x}}_{2 1,2}$...	$\hat{\mathbf{x}}_{k k}$...	$\hat{\mathbf{x}}_{q q}$
Forward-Backward Smoother (FBS)	$\hat{\mathbf{x}}_{1 1}$	$\hat{\mathbf{x}}_{2 1,2}$...	$\hat{\mathbf{x}}_{k k}$...	$\hat{\mathbf{x}}_{q q}$
						\vdots
						$\hat{\mathbf{x}}_{1 Q}$

Fig. 2 Three Estimation Methods Used To Investigate Sequential RAIM

We use the notation:

$$\mathbf{z}_Q = [\mathbf{z}_1^T \quad \cdots \quad \mathbf{z}_q^T]^T$$

The same notation is used for \mathbf{H}_Q and for $\boldsymbol{\varepsilon}_Q$. The batch implementation can accommodate any type of state propagation dynamics, which is included in the structure and coefficients of \mathbf{H}_Q and in the distribution of $\boldsymbol{\varepsilon}_Q$. There is usually more than one way to obtain equivalent batch realizations (see Appendix for example realizations, including a compact batch estimator and a reduced-order batch residual formulation).

In all linear batch realizations, a single measurement equation 14 can be obtained, which is expressed as:

$$\mathbf{z}_Q = \mathbf{H}_Q \mathbf{x}_Q + \boldsymbol{\varepsilon}_Q \quad (15)$$

Equations 1 to 11 apply to the batch implementation 15. For example, the RAIM residual in equation 8 applied to the batch becomes:

$$\mathbf{r}_{Q|Q} \equiv \mathbf{z}_Q - \mathbf{H}_Q \hat{\mathbf{x}}_{Q|Q}$$

The vector $\mathbf{r}_{Q|Q}$ includes residual components at each epoch, knowing all measurements:

$$\mathbf{r}_{Q|Q} = [\mathbf{r}_{1|Q}^T \quad \cdots \quad \mathbf{r}_{q|Q}^T]^T \quad (16)$$

The weighted norm of $\mathbf{r}_{Q|Q}$ is given by:

$$\|\mathbf{r}_{Q|Q}\|_W^2 = \mathbf{r}_{Q|Q}^T \mathbf{V}_Q^{-1} \mathbf{r}_{Q|Q} \quad (17)$$

where \mathbf{V}_Q is the covariance matrix of $\boldsymbol{\varepsilon}_Q$ (akin to equation 2). Let m_k and n_k respectively be the numbers of states and measurements at epoch k (and m_K and n_K are the corresponding numbers over epochs 1 to k). We have:

$$\|\mathbf{r}_{Q|Q}\|_W^2 \sim nc\chi^2(n_Q - m_Q, \lambda_{Q|Q}^2)$$

$$\lambda_{Q|Q}^2 = \mathbf{f}_Q^T \mathbf{V}_Q^{-1} (\mathbf{I} - \mathbf{H}_Q \mathbf{S}_Q) \mathbf{f}_Q$$

where

$$\mathbf{S}_Q = (\mathbf{H}_Q^T \mathbf{V}_Q^{-1} \mathbf{H}_Q)^{-1} \mathbf{H}_Q^T \mathbf{V}_Q^{-1}$$

Batch RAIM is effective (see for example, [17]), but it sets demanding computation and memory requirements (for the storage and processing of past-time measurements and state coefficients). In response, a computationally efficient FBS RAIM procedure is devised.

Forward-Backward Smoother RAIM Weighted Residual Generation

Significant improvement in batch processing efficiency was achieved in [16] using a sparse matrix block Cholesky decomposition algorithm for carrier phase positioning. However, this procedure lacked flexibility when handling satellite signals coming in and out of sight of the user antenna. As an alternative, a fixed interval smoother was proposed in [14], which may be

implemented using a FBS or a Rauch-Tung-Striebel smoother [18].

The associated RAIM residual generation process follows from the residual definition (in equation 8). For consistency of notation with the batch RAIM method, FBS state estimates $\hat{\mathbf{x}}_{k|Q}$ and residual vector components $\mathbf{r}_{k|Q}$ at any epoch k are expressed in terms of batch observation matrices \mathbf{H}_k and \mathbf{H}_Q and of batch measurement noise covariance matrices \mathbf{V}_k and \mathbf{V}_Q . At current time t_q (after the forward filter was completed), each iteration k of the backward smoother produces a state estimate $\hat{\mathbf{x}}_{k|Q}$ from which the k^{th} residual component is derived:

$$\mathbf{r}_{k|Q} = \mathbf{z}_k - \mathbf{H}_k \hat{\mathbf{x}}_{k|Q} \quad (18)$$

The norm of \mathbf{r}_k weighted by the measurement noise information matrix \mathbf{V}_k^{-1} is given by:

$$\|\mathbf{r}_{k|Q}\|_W^2 = \mathbf{r}_{k|Q}^T \mathbf{V}_k^{-1} \mathbf{r}_{k|Q} \quad (19)$$

In the presence of time-uncorrelated measurement noise, the batch measurement noise covariance matrix \mathbf{V}_Q is block diagonal, with diagonal matrices $\mathbf{V}_1 \dots \mathbf{V}_q$. In this case, the weighted squared norm of the batch that is equivalent to equation 17 can be directly computed as:

$$\|\mathbf{r}_{Q|Q}\|_W^2 = \sum_{k=Q} \|\mathbf{r}_{k|Q}\|_W^2 \quad (20)$$

However, accounting for time-correlated measurement noise (i.e., \mathbf{V}_Q not being block-diagonal) requires an additional residual weighting process. This process is derived in Appendix for measurement error dynamics encountered in actual carrier phase positioning problems [17]: the total FBS test statistic comprises contributions from uncorrelated measurement noise $\|\mathbf{r}_{QB}\|_{RN}^2$ (corresponding to receiver noise), from correlated measurement noise $\|\mathbf{r}_{MP}\|_{MP}^2$ (e.g., due to multipath) and from prior knowledge on constant state variables $\|\mathbf{r}_{PK}\|_{PK}^2$ (e.g., corresponding to bounding values on distributions of constant error parameters, including spacecraft clock and orbit and tropospheric biases and gradients). The final result, consistent with the batch RAIM implementation, is expressed as:

$$\|\mathbf{r}_{Q|Q}\|_W^2 = \|\mathbf{r}_{QB}\|_{RN}^2 + \|\mathbf{r}_{MP}\|_{MP}^2 + \|\mathbf{r}_{PK}\|_{PK}^2$$

This residual weighting procedure does not require any extra matrix inversion so that the FBS RAIM method remains computationally efficient.

For real-time applications with limited memory and computation capacity, the FBS residual-based RAIM method might still be insufficient. This is why a Kalman filter implementation is investigated in the next section.

V. KALMAN FILTER RAIM RESIDUAL

This section describes the derivation of a truly sequential KF residual-based RAIM method in presence of time-uncorrelated measurement noise.

At each epoch k of the filtering time-sequence (that spans from the initial epoch 1 to the current epoch q), the KF provides a state estimate $\hat{\mathbf{x}}_{k|K}$ and a residual vector component $\mathbf{r}_{k|K}$. For consistency of notation with the previously derived batch RAIM method, $\hat{\mathbf{x}}_{k|K}$ and $\mathbf{r}_{k|K}$ are given in terms of batch observation and measurement noise covariance matrices \mathbf{H}_k and \mathbf{V}_k , respectively. In addition, in this paragraph, $\hat{\mathbf{x}}_{k|K}$ and $\mathbf{r}_{k|K}$ are expressed assuming a batch estimator from epoch 1 to k (the next paragraphs go back to comparisons with the full batch estimator between epochs 1 and q). The state estimate and residual vectors are given by:

$$\hat{\mathbf{x}}_{k|K} = \mathbf{S}_K \mathbf{z}_K \quad (21)$$

$$\mathbf{r}_{k|K} \equiv \mathbf{z}_k - \mathbf{H}_k \hat{\mathbf{x}}_{k|K} \quad (22)$$

where $\mathbf{S}_K = (\mathbf{H}_K^T \mathbf{V}_K^{-1} \mathbf{H}_K)^{-1} \mathbf{H}_K^T \mathbf{V}_K^{-1}$ (23)

$$\mathbf{H}_K = [\mathbf{H}_1^T \quad \dots \quad \mathbf{H}_k^T]^T,$$

$$\mathbf{z}_K = [\mathbf{z}_1^T \quad \dots \quad \mathbf{z}_k^T]^T$$

and

$$\mathbf{V}_K = \begin{bmatrix} \mathbf{V}_1 & & \mathbf{0} \\ & \ddots & \\ \mathbf{0} & & \mathbf{V}_k \end{bmatrix}$$

Let $\mathbf{T}_{k|K}$ be a $n_k \times n_K$ transformation matrix (made of zeros and ones) that extracts measurements at epoch k from the batch measurement vector \mathbf{z}_K . The measurement vector \mathbf{z}_k can be expressed as:

$$\mathbf{z}_k = \mathbf{T}_{k|K} \mathbf{z}_K \quad (24)$$

and equation 22 becomes:

$$\mathbf{r}_{k|K} = (\mathbf{T}_{k|K} - \mathbf{H}_k \mathbf{S}_K) \mathbf{z}_K \quad (25)$$

As mentioned in Section III, current time state estimates $\hat{\mathbf{x}}_{q|Q}$ are identical for the batch and KF. It follows that current-time residual components are identical as well:

$$\mathbf{r}_{q|Q} \equiv \mathbf{z}_q - \mathbf{H}_q \hat{\mathbf{x}}_{q|Q} \quad (26)$$

This is the same observation as in equation 18 for the FBS. However for the KF, it is only true at the current-time epoch q . At previous epochs, the KF state estimate

vector $\hat{\mathbf{x}}_{k|K}$ differs from the full batch estimate $\hat{\mathbf{x}}_{k|Q}$. We first discuss the current-time residual component $\mathbf{r}_{q|Q}$ and then previous components $\mathbf{r}_{k|K}$.

Current-Time Kalman Filter RAIM Residual Component

The problem statement in Section III emphasizes that random parts of the test statistic and state estimates should be independent to enable P_{MD} computation using equation 12. In this regard, the current-time KF residual vector component $\mathbf{r}_{q|Q}$ in equation 26 can be expressed as a function of the batch residual vector $\mathbf{r}_{Q|Q}$ (known to lay in the parity space of \mathbf{H}_Q):

$$\mathbf{r}_{q|Q} = \mathbf{T}_{q|Q} \mathbf{r}_{Q|Q} = \begin{bmatrix} \mathbf{0} & \mathbf{I} \end{bmatrix} \mathbf{r}_{Q|Q} \quad (27)$$

It means that the vector $\mathbf{r}_{q|Q}$ is included in a subspace of the parity space of \mathbf{H}_Q from which $\hat{\mathbf{x}}_{q|Q}$ is derived. Therefore, the random part of the current-time KF residual component $\mathbf{r}_{q|Q}$ is statistically independent from $\hat{\mathbf{x}}_{q|Q}$. The weighted norm of $\mathbf{r}_{q|Q}$ is defined as:

$$\|\mathbf{r}_{q|Q}\|_W^2 = \mathbf{r}_{q|Q}^T \mathbf{V}_q^{-1} \mathbf{r}_{q|Q} \quad (28)$$

It is used to compute the KF RAIM test statistic.

Past-Time Kalman Filter RAIM Residual Components

In the same way as for the state estimates ($\hat{\mathbf{x}}_{k|K}$ and $\hat{\mathbf{x}}_{k|Q}$), past-time residual components for the batch ($\mathbf{r}_{k|Q}$) and for the KF ($\mathbf{r}_{k|K}$) differ. The KF residual vector component $\mathbf{r}_{k|K}$ in 25 can be expressed in terms of the full batch measurement vector \mathbf{z}_Q :

$$\mathbf{r}_{k|K} = \mathbf{M}_{k|Q} \mathbf{z}_Q$$

where $\mathbf{M}_{k|Q} = \begin{bmatrix} \mathbf{T}_{k|K} & \mathbf{0} \end{bmatrix} - \mathbf{H}_k \begin{bmatrix} \mathbf{S}_K & \mathbf{0} \end{bmatrix}$

The random parts of $\mathbf{r}_{k|K}$ and $\hat{\mathbf{x}}_{q|Q}$ are derived from orthogonal components of \mathbf{z}_Q if:

$$\mathbf{M}_{k|Q} \mathbf{H}_Q = \mathbf{0} \quad (29)$$

Proof of the previous statement is explained as follows. Let \mathbf{z}_0 be any n_Q -dimensional vector belonging to the range of \mathbf{H}_Q (i.e., laying in the state space). Vector \mathbf{z}_0 is a linear combination of columns of \mathbf{H}_Q that can be expressed as $\mathbf{H}_Q \delta \mathbf{x}_0$, where $\delta \mathbf{x}_0$ is a m_Q -dimensional vector. Let \mathbf{r}_0 be the residual vector computed using \mathbf{z}_0 :

$$\mathbf{r}_0 = \mathbf{M}_{k|Q} \mathbf{z}_0 = \mathbf{M}_{k|Q} \mathbf{H}_Q \delta \mathbf{x}_0$$

If \mathbf{r}_0 and $\delta \mathbf{x}_0$ are derived from orthogonal components of \mathbf{z}_0 for any \mathbf{z}_0 (with $\mathbf{z}_0 = \mathbf{H}_Q \delta \mathbf{x}_0$), then \mathbf{r}_0 must equal

zero for any $\delta \mathbf{x}_0$, which means that equation 29 must be satisfied. Equation 29 is satisfied since

$$\begin{bmatrix} \mathbf{T}_{k|K} & \mathbf{0} \end{bmatrix} \mathbf{H}_Q = \mathbf{H}_k$$

and

$$\begin{bmatrix} \mathbf{S}_K & \mathbf{0} \end{bmatrix} \mathbf{H}_Q = \mathbf{S}_K \mathbf{H}_K = \mathbf{I}.$$

Therefore, residual components $\mathbf{r}_{k|K}$ are statistically independent from $\hat{\mathbf{x}}_{q|Q}$ and can contribute to the KF test statistic.

Kalman Filter RAIM Test-Statistic Definition

In this early stage of the research, only the current-time KF residual component $\mathbf{r}_{q|Q}$ (identical to the current-time batch component) was considered for the KF RAIM test statistic. In future work, past-time residual components will be included as well. It is noteworthy that KF innovations, which are commonly implemented as detection test statistics, are statistically dependent on the state estimate and can not be used in RAIM-type procedures requiring P_{MD} computation following equation 12.

Therefore in this paper, the KF RAIM test statistic is the weighted norm $\|\mathbf{r}_{q|Q}\|_W^2$ defined in equation 28. Using equations 17, 26 and 27, $\|\mathbf{r}_{q|Q}\|_W^2$ is expressed as:

$$\|\mathbf{r}_{q|Q}\|_W^2 = \mathbf{z}_Q^T \mathbf{A}_{q|Q} \mathbf{z}_Q$$

where $\mathbf{A}_{q|Q} = (\mathbf{I} - \mathbf{H}_Q \mathbf{S}_Q)^T \begin{bmatrix} \mathbf{0} & \mathbf{0} \\ \mathbf{0} & \mathbf{V}_q^{-1} \end{bmatrix} (\mathbf{I} - \mathbf{H}_Q \mathbf{S}_Q)$

The norm $\|\mathbf{r}_{q|Q}\|_W^2$ is a quadratic form of the non-zero mean normally distributed measurement vector \mathbf{z}_Q . It is also a component of the batch RAIM residual test statistic $\|\mathbf{r}_{Q|Q}\|_W^2$ (which follows a non-central chi square distribution with $n_Q - m_Q$ degrees of freedom):

$$\|\mathbf{r}_{Q|Q}\|_W^2 = \|\mathbf{r}_{q|Q}\|_W^2 + \sum_{k=Q-1} \|\mathbf{r}_{k|Q}\|_W^2$$

From these observations, we make the conjecture that $\|\mathbf{r}_{q|Q}\|_W^2$ follows a *generalized non-central chi-square distribution* [19] [20], whose probability density function is given by:

$$f_{\|\mathbf{r}_{q|Q}\|_W^2}(x; k, \lambda^2) = \frac{1}{2} e^{-(x+\lambda^2)/2} \left(\frac{x}{\lambda^2} \right)^{k/4-1/2} I_{k/2-1}(\lambda \sqrt{x})$$

with parameters:

$$k = (n_Q - m_Q) \frac{n_q}{n_Q}$$

$$\lambda^2 = \lambda_{q|Q}^2 = \mathbf{f}_Q^T (\mathbf{I} - \mathbf{H}_Q \mathbf{S}_Q)^T \mathbf{T}_{q|Q}^T \mathbf{V}_{q|Q}^{-1} \mathbf{T}_{q|Q} (\mathbf{I} - \mathbf{H}_Q \mathbf{S}_Q) \mathbf{f}_Q$$

and where $I_v(z)$ is a modified Bessel function of the first kind. This conjecture will be demonstrated in a forthcoming paper. It was verified numerically assuming time-uncorrelated normally distributed measurement noise.

The Kalman filter test statistic $\|\mathbf{r}_{q|Q}\|_W^2$ can be used independently at each current-time epoch to compute the probability of missed detection P_{MD} (equation 12). Taking credit for previous integrity checks is not a viable solution for continuous operation (it would imply allocating requirements between an increasingly large number of epochs and accounting for undetected, tolerable faults at all previous time updates).

At this point in the paper, given that the batch and KF test statistics follow two different probability distributions, direct comparison is not trivial. In Section VII, availability performance comparisons between batch and KF implementations are carried out for a same sequence of measurements.

VI. IMPACT OF THE BATCH SAMPLING INTERVAL

The batch sampling interval T_{SB} of stored past-time measurements is a navigation system design parameter that can be modified with the batch, but not with the KF implementation. (The sampling interval T_{SB} within the batch does not need to be the same as the positioning update period T_{PU} .) Increasing T_{SB} lowers the least-squares batch estimation performance but also reduces the computational and memory load. This section analyzes the impact of T_{SB} on the fault-detection performance.

Referring back to Fig. 1, sensitivity to T_{SB} is first investigated on the joint distribution (represented by the ellipse, assuming a fixed point on the two-dimensional δx -versus- $\|\mathbf{r}\|_W$ plane) and then, on the slope parameter.

Impact on the Joint Distribution

Consider a fixed point on the plane, defined by the mean μ_t of δx and the non-centrality parameter λ_t of $\|\mathbf{r}\|_W$. A smaller sampling interval T_{SB} yields a larger number of batch measurements n_Q . As illustrated in Fig. 3, the resulting increased estimation performance is represented by a reduction along the vertical direction of the ellipse of constant joint-probability. A smaller T_{SB} also causes a larger number of degrees of freedom $n_Q - m_Q$ of the non-centrally chi-square distributed $\|\mathbf{r}\|_W$ (horizontal axis).

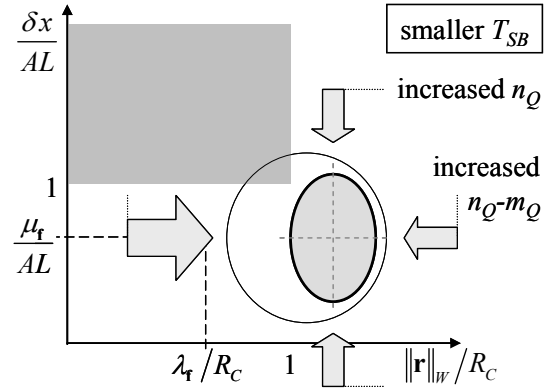


Fig. 3 Failure Mode Slope Plot for a Lower Sampling Interval

To investigate the impact of smaller T_{SB} on $\|\mathbf{r}\|_W$, Fig. 4 presents chi-square cumulative distribution functions (CDF) and probability density functions (PDF) for numbers of degrees of freedom (NDOF) ranging from 1 to 10. In the upper plot of Fig. 4, chi-square CDFs are displayed over a normalized x-axis. All curves intercept at the probability percentile selected for the normalizing threshold. A percentile value of 0.5 was selected for illustrative purposes (the corresponding percentile used in RAIM is $1 - P_C$). To the left of the threshold, the lowest curves correspond to the highest NDOF. This observation remains true for non-central chi-square CDFs with fixed normalized non-centrality parameters. It means that smaller sampling intervals T_{SB} (i.e., higher NDOF) will yield lower probabilities of no detection.

In addition, chi-square PDFs are plotted in the lower graph of Fig. 4. For constant probability density values, the spread of the distribution over the normalized x-axis narrows and slightly shifts to the right as NDOF increases. In terms of the ellipse representation in Fig. 3, smaller sampling intervals T_{SB} (larger NDOF) cause contours of constant joint-probability to shrink along the horizontal direction and to move rightwards, away from the missed-detection area.

Therefore, for a fixed point on the plot, decreasing the sampling interval T_{SB} reduces the probability of missed-detection P_{MD} . However, modifying T_{SB} also impacts the mean μ_t of δx and the non-centrality parameter λ_t of $\|\mathbf{r}\|_W$, the ratio of which is the *slope* parameter. The next subsection analyzes T_{SB} versus *slope*, in the presence of correlated measurement noise.

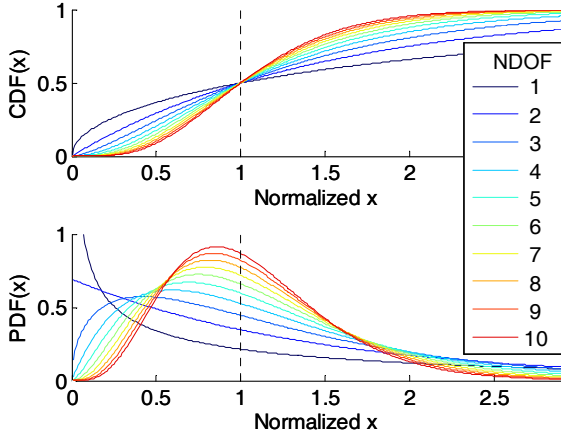


Fig. 4 Chi-Square CDFs and PDFs Over Normalized X-Axis for Varying Numbers of Degrees of Freedom

Impact on the Slope Parameter

To illustrate the impact of the sampling interval T_{SB} on the *slope* parameter, a simple one-dimensional example is considered where the state x is a constant scalar over two epochs (1 and 2). The measurement equation is:

$$\mathbf{z} = \mathbf{H}\mathbf{x} + \mathbf{v} + \mathbf{f}$$

where $\mathbf{z} = [z_1 \ z_2]^T$, $\mathbf{H} = [h_1 \ h_2]^T$
 $\mathbf{v} = [v_1 \ v_2]^T$ and $\mathbf{f} = [f_1 \ f_2]^T$

The measurement noise vector is defined as:

$$\mathbf{v} \sim \mathcal{N}(\mathbf{0}, \mathbf{V})$$

with:

$$\mathbf{V} = \sigma^2 \begin{bmatrix} 1 & \eta \\ \eta & 1 \end{bmatrix}$$

The correlation coefficient η for a Gauss-Markov process (GMP) is expressed as:

$$\eta = e^{-T_{SB}/T_{MP}} \sigma^2 \quad (30)$$

where T_{MP} is the GMP correlation time constant.

For this one-dimensional case, the mean μ_t of the estimate error δx (defined in equation 7) has a simple expression:

$$\mu_t = \frac{f_1 h_1 + f_2 h_2 - (f_2 h_1 + f_1 h_2) \eta}{h_1^2 - 2h_1 h_2 \eta + h_2^2}$$

Because of the term in η , the sign of δx depends on the relative values of state and fault coefficients (h_i and f_i) (the denominator is always positive because $\eta < 1$). The non-centrality parameter λ_r^2 of the residual's weighted norm $\|\mathbf{r}\|_w^2$ (equation 11) is expressed as:

$$\sqrt{\lambda_r^2} = \frac{|f_1 h_2 - f_2 h_1|}{\sigma \sqrt{h_1^2 - 2h_1 h_2 \eta + h_2^2}}$$

Finally, the normalized *slope* parameter represented in Fig. 1 is defined as:

$$\text{slope} \equiv \frac{|\mu_t| R_C}{\lambda_r AL}$$

$$\text{slope} = \sigma \frac{|f_1 h_1 + f_2 h_2 - (f_1 h_2 + f_2 h_1) \eta| R_C}{|f_1 h_2 - f_2 h_1| \sqrt{h_1^2 + h_2^2 - 2h_1 h_2 \eta} AL} \quad (31)$$

The denominator of *slope* corroborates a known result: if \mathbf{H} and \mathbf{f} are parallel (if their cross-product is null), the fault can not be detected (infinite *slope*); \mathbf{f} is entirely transformed from the measurement space to the state space through the weighted pseudo-inverse of \mathbf{H} .

However, if \mathbf{f} is orthogonal to the columns of \mathbf{H} (if their dot-product is null), the numerator does not go to zero (which would mean no impact on δx) due the correlation term in η . Furthermore, the absolute value in the numerator causes the *slope* parameter to have a minimum (when it cancels) that is a function of η . The value of η that causes the slope to be null (and hence that minimizes the impact on δx) is given by:

$$\eta = \frac{f_1 h_1 + f_2 h_2}{f_1 h_2 + f_2 h_1}$$

The corresponding sampling interval value is (from equation 30):

$$T_{SB} = \ln \left(\frac{f_1 h_2 + f_2 h_1}{f_1 h_1 + f_2 h_2} \right) T_{MP} \quad (32)$$

This last expression reveals a counter-intuitive result: in the presence of time-correlated measurement noise, the value of the sampling interval T_{SB} that maximizes RAIM detection performance is not necessarily zero (it depends on state and fault coefficients, and on T_{MP}).

This observation may be exploited in case of repeated measurement geometries and fault profiles by selecting the sampling interval that maximizes the overall performance.

Combining this result with the conclusion of the previous subsection shows that the sampling interval T_{SB} exercises conflicting influences on the fault-detection performance. To assess the overall impact of T_{SB} on a realistic multi-dimensional navigation system, performance evaluations are carried out.

VII. PERFORMANCE ANALYSIS

Availability Analysis for Aircraft Precision Approach

The performance analysis is structured around the benchmark application of aircraft precision approach, where an airplane flies toward a runway at a constant 70 m/s velocity, along a constant 3 deg glide slope angle. Code and carrier phase GPS and Galileo measurements collected over a 5 min smoothing period T_{SW} are used in the estimation and detection algorithms. To account for various satellite geometries, approaches starting at regular 1 min intervals are considered over a 10 day period (10 days is the combined GPS/Galileo constellation repeatability period [12]). The percentage of approaches that meets the integrity requirement (in equation 13) over the total number of simulated approaches is the measure of fault-detection performance or RAIM availability.

It is further assumed that the user has real-time access to measurements from a nearby reference station. At each epoch k , differential code ρ_k and carrier phase ϕ_k measurements for all satellites are stacked together in a measurement vector:

$$\begin{bmatrix} \rho_k \\ \phi_k \end{bmatrix} = \begin{bmatrix} \mathbf{G} & 1 & \mathbf{0} \\ \mathbf{G} & 1 & \mathbf{I} \end{bmatrix} \begin{bmatrix} \mathbf{x}_{U,k} \\ \tau_k \\ \mathbf{n} \end{bmatrix} + \begin{bmatrix} \mathbf{v}_{\rho,k} \\ \mathbf{v}_{\phi,k} \end{bmatrix} \quad (33)$$

where \mathbf{G} is the satellite geometry matrix, $\mathbf{x}_{U,k}$ is the user position (in a local reference frame, with respect to the reference station location), τ_k is the differential receiver clock bias and \mathbf{n} is the vector of differenced cycle ambiguities. The code and carrier phase measurement noise vectors are respectively defined as:

$$\mathbf{v}_{\rho,k} \sim \mathbf{N}(\mathbf{0}, \mathbf{I}\sigma_{\rho}^2) \quad \text{and} \quad \mathbf{v}_{\phi,k} \sim \mathbf{N}(\mathbf{0}, \mathbf{I}\sigma_{\phi}^2)$$

Measurement faults (not expressed in equation 33) include ramp-type and step-type failure mode profiles of all starting times and magnitudes [12].

The next two subsections will include comparative performance evaluations. Therefore, values given to the error model and to the navigation requirements are not meant to predict actual system performance, but rather to provide a framework for comparative analyses. The assumed differential measurement receiver noise and multipath noise standard deviations for code and carrier phase are respectively:

$$\sigma_{\rho} = 1.57 \text{ m} \quad \text{and} \quad \sigma_{\phi} = 1.6 \text{ cm}.$$

In the example application of aircraft approach, the main focus is on the vertical position coordinate (requirements are often more stringent along the vertical direction than along the horizontal). Navigation requirements include a vertical alert limit or VAL of 10 m, a continuity risk requirement P_C of $8 \cdot 10^{-6}$, an integrity requirement P_{HMI}

of 10^{-7} and we assume a prior probability of fault P_p of $2.5 \cdot 10^{-5}$ (failure rate of 10^{-4} /hr over 15min exposure periods).

Batch RAIM Performance Sensitivity to Sampling Interval

To illustrate and corroborate the result of the analysis in Section VI, availability performance sensitivity to the batch sampling interval T_{SB} is quantified in presence of measurement error time-correlation. In this subsection, the vectors \mathbf{v}_{ρ} and \mathbf{v}_{ϕ} are time correlated. The vector \mathbf{v}_{ρ} has a time-uncorrelated part $\mathbf{v}_{RN,\rho}$ (caused by receiver noise) and a time-correlated part $\mathbf{v}_{MP,\rho}$ (due to multipath) modeled as a first order GMP with time constant T_{MP} :

$$\mathbf{v}_{\rho} = \mathbf{v}_{RN,\rho} + \mathbf{v}_{MP,\rho}$$

$$\mathbf{v}_{RN,\rho} \sim \mathbf{N}(\mathbf{0}, \mathbf{I}\sigma_{RN,\rho}^2)$$

$$\text{and} \quad \mathbf{v}_{MP,\rho,k+1} = e^{-T_{SB}/T_{MP}} \mathbf{v}_{MP,\rho,k} + \xi_{MP,\rho,k} \quad (34)$$

$$\xi_{MP,\rho,k} \sim \mathbf{N}(\mathbf{0}, \mathbf{I}(1 - e^{-2T_{SB}/T_{MP}})\sigma_{MP,\rho}^2). \quad (35)$$

assuming:

$$\sigma_{RN,\rho} = 0.45 \text{ m} \quad \text{and} \quad \sigma_{M,\rho} = 1.5 \text{ m}.$$

The same model is employed for the carrier phase measurement noise vector \mathbf{v}_{ϕ} , with:

$$\sigma_{RN,\phi} = 0.5 \text{ cm} \quad \text{and} \quad \sigma_{M,\phi} = 1.5 \text{ cm}.$$

In Fig. 5, RAIM availability at the San Antonio, Texas location (near-worst location over CONUS) is plotted versus sampling interval T_{SB} for a fixed correlation time constant T_{MP} of 1 min. Maximum performance is achieved for T_{SB} values larger than 30s, but availability drops for smaller sampling intervals, down to 98.2% for a 5 s T_{SB} .

Fig. 5 confirms the counter-intuitive result captured in equation 32. In the presence of time-correlated measurement noise, smaller sampling intervals yield better estimation performance, but do not necessarily generate improved fault-detection performance. If the step and ramp-type failures used to establish Fig. 5 actually represent realistic fault modes, the sampling interval T_{SB} should be selected larger than 30 s to maximize detection performance (which, incidentally, lowers the computational load as compared to smaller T_{SB} -values).

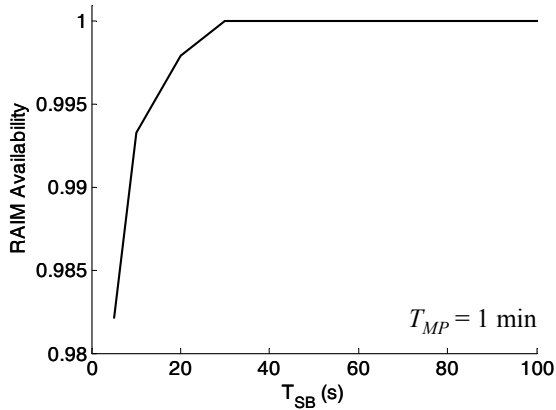


Fig. 5 Performance Sensitivity to Sampling Interval Assuming a 1-min Correlation Time Constant

Performance Comparison between Batch and KF RAIM Methods over CONUS

The performance of the batch and KF RAIM methods are evaluated for a 5deg×5deg latitude-longitude grid of locations over CONUS. The same sequence of measurements is used for both algorithms. In this subsection, the vectors \mathbf{v}_ρ and \mathbf{v}_ϕ are time-uncorrelated random sequences.

Fig. 6 shows availability maps for the batch RAIM method and for the KF implementation. RAIM availability is color-coded: white color corresponds to 100%, black corresponds to 96%. The batch RAIM method (perfect availability at all locations) clearly performs better than the KF procedure (availability ranges between 96% and 100%), but at the expense of more demanding computation and memory requirements. Still, for the set of benchmark navigation requirements and error models considered here, high performance is achieved in many locations of the KF RAIM availability map. The KF-based method provides fault-detection capability and is a viable solution, especially in applications with limited memory and computation resources.

VIII. CONCLUSION

This paper introduced two RAIM-based procedures for navigation systems that require measurement filtering over time. First, a computationally efficient batch-type weighted residual generation process was established using a forward-backward smoother. It accounts for time-correlated measurement noise and for prior knowledge on state variables. Second, a KF RAIM test-statistic was defined using the current-time component of the KF residual.

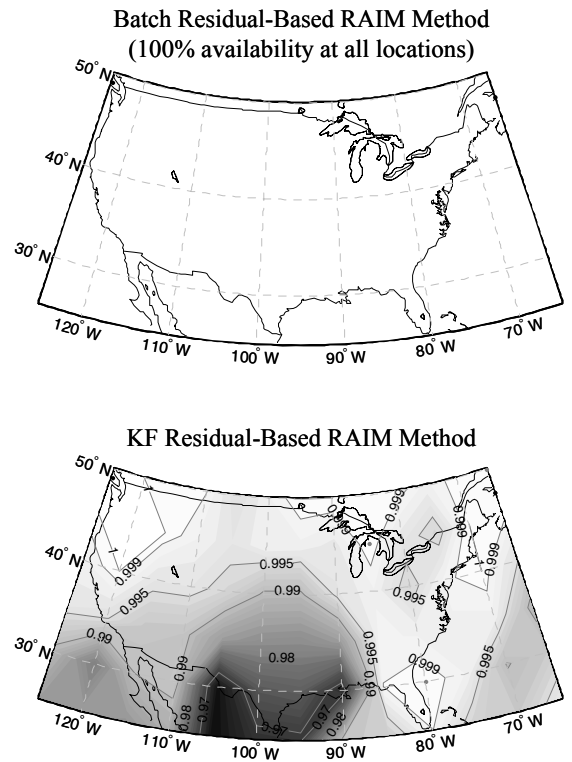


Fig. 6 Availability Maps for the Batch and KF RAIM Methods

Performance evaluations show that the batch RAIM algorithm performs better than the KF implementation, at the expense of more demanding processing and memory requirements. The truly sequential KF residual-based RAIM method is better suited to applications with limited computation resources. For the batch RAIM method, the paper showed that increasing the batch sampling interval to reduce the computation load may also improve the detection performance (depending on measurement error correlation and fault profiles).

Future developments of the KF residual based RAIM algorithm, including weighting of the test statistic in the presence of correlated measurement noise and inclusion of past-time KF residual contributions, will widen the scope of applicability of the method and enhance the KF RAIM performance.

APPENDIX

In this appendix, a method is established to compute the weighted norm of the FBS residual. The most challenging aspect of the derivation is to correctly account for measurement error time-correlation and for prior knowledge of constant state variables. This type of

measurement error dynamics are encountered in carrier phase-based navigation systems (e.g., [11]).

Reduced-Order Batch RAIM Formulation Including Prior Knowledge and Correlated Measurement Noise

The batch measurement equation 15 is rewritten as:

$$\mathbf{z}_Q = \mathbf{H}_Q \mathbf{x}_Q + \mathbf{v}_Q + \mathbf{f}_Q \quad (36)$$

Components of the measurement error model are broken down in three parts (prior knowledge on state variables, time-unrelated and time-correlated measurement noise) in order to explain the weighting of the RAIM residual's norm. Therefore \mathbf{v}_Q in equation 36 is replaced by $\mathbf{v}_{RN} + \mathbf{v}_{other}$. The vector \mathbf{v}_{other} serves as place-holder for time-correlated terms that are added in the next paragraphs.

$$\mathbf{z}_Q = \mathbf{H}_Q \mathbf{x}_Q + \mathbf{v}_{RN} + \mathbf{v}_{other} + \mathbf{f}_Q$$

The time-unrelated measurement noise vector \mathbf{v}_{RN} corresponding to receiver noise (RN) is defined as:

$$\mathbf{v}_{RN} \sim \mathcal{N}(\mathbf{0}, \mathbf{V}_{RN})$$

where the covariance matrix \mathbf{V}_{RN} is diagonal.

Prior knowledge (PK) on constant state variables \mathbf{x}_{PK} can be included using a pseudo-measurement vector \mathbf{z}_{PK} :

$$\mathbf{z}_{PK} = \mathbf{H}_{PK} \mathbf{x}_{PK} + \mathbf{v}_{PK} \quad (37)$$

where the covariance matrix \mathbf{V}_{PK} of \mathbf{v}_{PK} comprises bounding values on state parameter distributions. For example, an extra state may be included to account for a constant tropospheric error gradient. If this gradient's distribution is known to be bounded by a Gaussian function (e.g., from experimental analysis), the standard deviation of that bounding Gaussian function is the prior knowledge to be incorporated. It is captured in \mathbf{V}_{PK} [11].

In addition, if measurement error time-correlation can be modeled as a first order GMP with time constant T_{MP} , the measurement vector can be expressed as in equations 34 and 35. Measurement error correlation in satellite signals is caused by multipath (MP). Consider a vector \mathbf{v}_{MP} of time-correlated measurement errors from epochs 1 to q ordered by measurement source (i.e., by satellite transmitter):

$$\mathbf{v}_{MP} \sim \mathcal{N}(\mathbf{0}, \mathbf{V}_{MP})$$

The covariance matrix \mathbf{V}_{MP} is block diagonal, with n_{SV} blocks, n_{SV} being the number of satellites:

$$\mathbf{V}_{MP} = \begin{bmatrix} \mathbf{V}_{MP} & \mathbf{0} \\ \mathbf{0} & \mathbf{V}_{MP} \\ \mathbf{0} & \mathbf{0} & \mathbf{V}_{MP} \end{bmatrix}$$

Each block corresponds to observations from a same satellite over time. Within each block ${}^k\mathbf{V}_{MP}$, the (i, j) th element of ${}^k\mathbf{V}_{MP}$ models the time-correlation between two measurements at sample times t_i and t_j as $\sigma_M^2 e^{-\Delta t_{ij}/T_M}$, where $\Delta t_{ij} = |t_i - t_j|$ [11]. Time-correlated measurement noise can be included using a pseudo-measurement vector \mathbf{z}_{MP} :

$$\mathbf{z}_{MP} = \mathbf{H}_{MP} \mathbf{x}_{MP} + \mathbf{v}_{MP} \quad (38)$$

Equations 37 and 38 assume that multipath states and states for which prior knowledge is available were not included in the original measurement equation 36. The complete batch measurement equation is given by:

$$\begin{bmatrix} \mathbf{z}_Q \\ \mathbf{z}_{PK} \\ \mathbf{z}_{MP} \end{bmatrix} = \begin{bmatrix} \mathbf{H}_Q & \mathbf{H}_{Q,PK} & \mathbf{H}_{Q,MP} \\ \mathbf{0} & \mathbf{H}_{PK} & \mathbf{0} \\ \mathbf{0} & \mathbf{0} & \mathbf{H}_{MP} \end{bmatrix} \begin{bmatrix} \mathbf{x}_Q \\ \mathbf{x}_{PK} \\ \mathbf{x}_{MP} \end{bmatrix} + \begin{bmatrix} \mathbf{v}_{RN} \\ \mathbf{v}_{PK} \\ \mathbf{v}_{MP} \end{bmatrix} + \begin{bmatrix} \mathbf{f}_Q \\ \mathbf{0} \\ \mathbf{0} \end{bmatrix} \quad (39)$$

It is worth noticing that the state vectors \mathbf{x}_{PK} and \mathbf{x}_{MP} are only incorporated in the estimator to model the measurement error model dynamics. They can be called nuisance parameters, and the parameters of interest (user positions and floating cycle ambiguities) are included in \mathbf{x}_Q . Equation 39 is written in a compact form:

$$\begin{bmatrix} \mathbf{z}_Q \\ \mathbf{z}_{PK} \\ \mathbf{z}_{MP} \end{bmatrix} = \begin{bmatrix} \mathbf{H}_{QB} \\ \mathbf{H}_{PKB} \\ \mathbf{H}_{MPB} \end{bmatrix} \mathbf{x}_B + \begin{bmatrix} \mathbf{v}_{RN} \\ \mathbf{v}_{PK} \\ \mathbf{v}_{MP} \end{bmatrix} + \begin{bmatrix} \mathbf{f}_Q \\ \mathbf{0} \\ \mathbf{0} \end{bmatrix} \quad (40)$$

We also use the notation:

$$\mathbf{z}_B = \mathbf{H}_B \mathbf{x}_B + \mathbf{v}_B + \mathbf{f}_B \quad (41)$$

The covariance matrix \mathbf{V}_B of \mathbf{v}_B is block diagonal, with \mathbf{V}_{RN} , \mathbf{V}_{PK} and \mathbf{V}_{MP} on the diagonal. Therefore, the covariance matrix \mathbf{P}_B of the least squares state estimate $\hat{\mathbf{x}}_B$ of \mathbf{x}_B is given by:

$$\mathbf{P}_B = (\mathbf{H}_B^T \mathbf{V}_B^{-1} \mathbf{H}_B)^{-1} \quad (42)$$

$$\mathbf{P}_B = (\mathbf{H}_{QB}^T \mathbf{V}_{RN}^{-1} \mathbf{H}_{QB} + \mathbf{H}_{PKB}^T \mathbf{V}_{PK}^{-1} \mathbf{H}_{PKB} + \mathbf{H}_{MPB}^T \mathbf{V}_{MP}^{-1} \mathbf{H}_{MPB})^{-1} \quad (43)$$

The estimate error $\delta \mathbf{x}_B$ is expressed as:

$$\delta \mathbf{x}_B = \mathbf{S}_B \mathbf{f}_B \quad (44)$$

where

$$\mathbf{S}_B = \mathbf{P}_B \mathbf{H}_B^T \mathbf{V}_B^{-1}$$

$\delta \mathbf{x}_B$ can be expressed in terms of the fault vector \mathbf{f}_Q as:

$$\delta \mathbf{x}_B = \mathbf{P}_B \mathbf{H}_{QB}^T \mathbf{V}_{RN}^{-1} \mathbf{f}_Q \quad (45)$$

In addition, the residual vector \mathbf{r}_B is written as:

$$\mathbf{r}_B = \begin{bmatrix} \mathbf{r}_{QB}^T & \mathbf{r}_{PK}^T & \mathbf{r}_{MP}^T \end{bmatrix}$$

Equation 8 yields:

$$\mathbf{r}_B \equiv \mathbf{z}_B - \mathbf{H}_B \hat{\mathbf{x}}_B$$

which results in:

$$\mathbf{r}_{QB} = \mathbf{f}_Q - \mathbf{H}_{QB} \mathbf{P}_B \mathbf{H}_{QB}^T \mathbf{V}_{RN}^{-1} \mathbf{f}_Q = \mathbf{f}_Q - \mathbf{H}_{QB} \delta \mathbf{x}_B \quad (46)$$

$$\mathbf{r}_{PK} = -\mathbf{H}_{PKB} \mathbf{P}_B \mathbf{H}_{QB}^T \mathbf{V}_{RN}^{-1} \mathbf{f}_Q = -\mathbf{H}_{PKB} \delta \mathbf{x}_B$$

$$\mathbf{r}_{MP} = -\mathbf{H}_{MPB} \mathbf{P}_B \mathbf{H}_{QB}^T \mathbf{V}_{RN}^{-1} \mathbf{f}_Q = -\mathbf{H}_{MPB} \delta \mathbf{x}_B$$

The last two equations can also be expressed in terms of state vector components using notations of equation 39:

$$\mathbf{r}_{PK} = -\mathbf{H}_{PK} \delta \mathbf{x}_{PK} \quad (47)$$

$$\mathbf{r}_{MP} = -\mathbf{H}_{MP} \delta \mathbf{x}_{MP} \quad (48)$$

Finally, the weighted norm squared of the batch residual is given by:

$$\|\mathbf{r}_B\|_W^2 = \mathbf{r}_B^T \mathbf{V}_B^{-1} \mathbf{r}_B \quad (49)$$

$$\|\mathbf{r}_B\|_W^2 = \mathbf{r}_{QB}^T \mathbf{V}_{RN}^{-1} \mathbf{r}_{QB} + \mathbf{r}_{PK}^T \mathbf{V}_{PK}^{-1} \mathbf{r}_{PK} + \mathbf{r}_{MP}^T \mathbf{V}_{MP}^{-1} \mathbf{r}_{MP} \quad (50)$$

We use the notations:

$$\|\mathbf{r}_{QB}\|_{RN}^2 = \mathbf{r}_{QB}^T \mathbf{V}_{RN}^{-1} \mathbf{r}_{QB} \quad (51)$$

$$\|\mathbf{r}_{PK}\|_{PK}^2 = \mathbf{r}_{PK}^T \mathbf{V}_{PK}^{-1} \mathbf{r}_{PK} \quad (52)$$

$$\|\mathbf{r}_{MP}\|_{MP}^2 = \mathbf{r}_{MP}^T \mathbf{V}_{MP}^{-1} \mathbf{r}_{MP} \quad (53)$$

Equations 50 to 53 show that the norm $\|\mathbf{r}_B\|_W^2$ can be broken down into a sum of three squared weighted norms with different weighting coefficients.

The expressions of \mathbf{P}_B in equation 43, of $\delta \mathbf{x}_B$ in equation 45 and of $\|\mathbf{r}_B\|_W^2$ in equation 50 are compact batch formulations that already improve the batch method efficiency (as compared to the original equations 42, 44 and 49, respectively). The iterative FBS is even more efficient, especially if the number of sample time-epochs is high.

FBS RAIM Residual Generation Process:

Each iteration of the backward smoother (corresponding to an epoch k) produces a state estimate vector $\hat{\mathbf{x}}_{B,k|Q}$ that can be used to compute a residual vector component $\mathbf{r}_{B,k|Q}$:

$$\mathbf{r}_{B,k|Q} = \begin{bmatrix} \mathbf{r}_{QB,k|Q} \\ \mathbf{r}_{PK,k|Q} \\ \mathbf{r}_{MP,k|Q} \end{bmatrix} = \mathbf{z}_{B,k} - \mathbf{H}_{B,k} \hat{\mathbf{x}}_{B,k|Q} \quad (54)$$

The residual weighting procedure is a two-step process. In a first step, following equations 51 and 52, weighted residual norm components at epoch k can be computed:

$$\|\mathbf{r}_{QB,k|Q}\|_{RN}^2 = \mathbf{r}_{QB,k|Q}^T \mathbf{V}_{RN}^{-1} \mathbf{r}_{QB,k|Q} \quad (55)$$

$$\|\mathbf{r}_{PK,k|Q}\|_{PK}^2 = \mathbf{r}_{PK,k|Q}^T \mathbf{V}_{PK}^{-1} \mathbf{r}_{PK,k|Q} \quad (56)$$

In addition, weighting elements of the residual corresponding time-correlated measurement noise $\mathbf{r}_{MP,k|Q}$ must account for correlation over time. One solution is simply to store the residual components $\mathbf{r}_{MP,k|Q}$ over the entire batch (while keeping track of satellite numbers). At the end of the smoothing process, the residual components can be regrouped per satellite. They can be weighted satellite per satellite, so that for a satellite i :

$$\|\mathbf{r}_{MP}\|_{MP}^2 = \mathbf{r}_{MP}^T \mathbf{V}_{MP}^{-1} \mathbf{r}_{MP} \quad (57)$$

The $q \times q$ weighting matrix \mathbf{V}_{MP}^{-1} can be computed off-line, and stored in a database (\mathbf{V}_{MP}^{-1} is fully defined by T_{SB} , T_{MP} and T_{SW}). Another solution is simply to consider a batch sampling interval T_{SB} larger than twice the multipath time constant T_{MP} to whiten the measurement noise; but other considerations may influence the choice of T_{SB} (see Section VI).

The second step of the residual weighting procedure occurs once the backward smoothing process has been completed. Since the uncorrelated measurement noise covariance matrix \mathbf{V}_{RN} is diagonal, the contribution of elements weighted by \mathbf{V}_{RN}^{-1} can be computed as:

$$\|\mathbf{r}_{QB}\|_{RN}^2 = \sum_{k=Q} \|\mathbf{r}_{QB,k|Q}\|_{RN}^2 \quad (58)$$

This case was presented in Section IV. Then, residual components weighted by the prior information matrix \mathbf{V}_{PK}^{-1} correspond to constant state coefficients (equation 47). The states $\mathbf{x}_{PK,k}$ appear in each FBS iteration, but their contribution should only be counted once. In order to deal with small changes in $\mathbf{r}_{PK,k|Q}$ due to satellites coming in and out of sight of the user antenna, we use the following expression:

$$\|\mathbf{r}_{PK}\|_{PK}^2 \approx \max_k \|\mathbf{r}_{PK,k|Q}\|_{PK}^2 \quad (59)$$

Finally, the contribution of residuals corresponding to time-correlated measurement errors can be summed up over all SVs (since \mathbf{V}_{MP} is block diagonal):

$$\|\mathbf{r}_{MP}\|_{MP}^2 = \sum_{i=1:n_S} \|\mathbf{r}_{MP}\|_{MP}^2 \quad (60)$$

Ultimately, following equations 50 to 53, the squared weighted norm of the residual over the entire batch is given by:

$$\|\mathbf{r}_{Q|Q}\|_W^2 = \|\mathbf{r}_{QB}\|_{RN}^2 + \|\mathbf{r}_{MP}\|_{MP}^2 + \|\mathbf{r}_{PK}\|_{PK}^2$$

REFERENCES

- [1] Lee, Y. C., "Analysis of Range and Position Comparison Methods as a Means to Provide GPS

- Integrity in the User Receiver,” *Proceedings of the 42nd Annual Meeting of The Institute of Navigation*, Seattle, WA, June 1986, pp. 1-4.
- [2] Parkinson, B. W., and Axelrad, P., “Autonomous GPS Integrity Monitoring Using the Pseudorange Residual,” *NAVIGATION*, Washington, DC, Vol. 35, No. 2, 1988, pp. 225-274.
- [3] Brown, R., “A Baseline RAIM Scheme and a Note on the Equivalence of Three RAIM Methods.” *NAVIGATION*. 39.4 (1992): 127-137.
- [4] Greenspan, R., “GPS and Inertial Integration,” *The Global Positioning System: Theory and Applications*, B. W. Parkinson, J. J. Spilker, Jr., P. Axelrad, P. Enge, editors, AIAA Progress in Aeronautics and Astronautics Volume 163-4, Washington, DC, 1996
- [5] Joerger, M., and Pervan, B., “Measurement-Level Integration of Carrier-Phase GPS and Laser-Scanner for Outdoor Ground Vehicle Navigation,” *ASME Journal of Dynamic Systems, Measurement, and Control*, Vol. 131, March 2009.
- [6] Chan, F-C., Joerger, M., Pervan, B., “High Integrity Stochastic Modeling of GPS Receiver Clock for Improved Positioning and Fault Detection Performance,” *Proceedings of IEEE/ION PLANS 2010*, Indian Wells, CA, May 2010, pp. 1245-1257.
- [7] Joerger, M., J. Christ, R. Duncan, and B. Pervan. “Integrated Design of an AGV for Improved GPS-based Path-Following Performance.” *International Journal of Vehicle Design*. 42.3/4 (2006): 263-286.
- [8] Clot, A., Macabiau, C., Nikiforov, I., Roturier, B., “Sequential RAIM Designed to Detect Combined Step Ramp Pseudo-Range Error,” *Proceedings of the 19th International Technical Meeting of the Satellite Division of The Institute of Navigation (ION GNSS 2006)*, Fort Worth, TX, September 2006, pp. 2621-2633.
- [9] Brown, R. G. and Hwang, Y. C., “GPS failure detection by autonomous means within the cockpit”, *Proceedings of the 42nd Annual Meeting of the Institute of Navigation*, Seattle, WA, June 1986, pp. 5-12.
- [10] Willsky, A., “A survey of design methods for failure detection in dynamic systems,” *Automatica*, Vol. 12, 1976, pp. 601-611.
- [11] Joerger, M., Neale, J., Pervan, B., “Iridium/GPS Carrier Phase Positioning and Fault Detection Over Wide Areas,” *Proceedings of the 22nd International Technical Meeting of The Satellite Division of the Institute of Navigation (ION GNSS 2009)*, Savannah, GA, September 2009, pp. 1371-1385.
- [12] Joerger, M., Neale, J., Pervan, B., Datta-Barua, S., “Measurement Error Models and Fault-Detection Algorithms for Multi-Constellation Navigation Systems,” *Proceedings of IEEE/ION PLANS 2010*, Indian Wells, CA, May 2010, pp. 927-946.
- [13] Sturza, M, “Navigation System Integrity Monitoring Using Redundant Measurements,” *NAVIGATION: Journal of the Institute of Navigation*, Washington, DC, Vol. 35 No. 4, 1988, pp. 69-87.
- [14] Pervan, B., “Navigation integrity for aircraft precision landing using the global positioning system,” *Ph.D. Dissertation*, Stanford University, March 1996.
- [15] Walter, T., and P. Enge, “Weighted RAIM for Precision Approach,” *Proceedings of the Institute of Navigation GPS Conference*, Palm Springs, CA, 1995.
- [16] Cohen, C. “Attitude Determination Using GPS,” *Ph.D. Dissertation*, Stanford University, December 1992.
- [17] Joerger, Mathieu, Gratton, Livio, Pervan, Boris, Cohen, Clark E., “Analysis of Iridium-Augmented GPS for Floating Carrier Phase Positioning”, *NAVIGATION*, Vol. 57, No. 2, Summer 2010, pp. 137-160.
- [18] Crassidis, J., and J. Junkins., *Optimal Estimation of Dynamic Systems*, Boca Raton, FL: Chapman & Hall/CRC, 2004.
- [19] Cacoullos, T. and Koutras, M., “Quadratic Forms in Spherical Random Variables: Generalized Noncentral χ^2 Distribution,” *Naval Research Logistics Quarterly*, Vol. 31, 1984, pp. 447-461.
- [20] Koutras, M., “On the Generalized Noncentral Chi-Squared Distribution Induced by an Elliptical Gamma Law,” *Biometrika*, Vol. 73, No. 2, 1986, pp. 528-532.